Continuous inertial focusing, ordering, and separation of particles in microchannels

Dino Di Carlo, Daniel Irimia, Ronald G. Tompkins, and Mehmet Toner*

BioMEMS Resource Center, Center for Engineering in Medicine and Surgical Services, Massachusetts General Hospital, Shriners Hospital for Children, and Harvard Medical School, Boston, MA 02114

Edited by Jerry P. Gollub, Haverford College, Haverford, PA, and approved October 8, 2007 (received for review May 25, 2007)

Under laminar flow conditions, when no external forces are applied, particles are generally thought to follow fluid streamlines. Contrary to this perspective, we observe that flowing particles migrate across streamlines in a continuous, predictable, and accurate manner in microchannels experiencing laminar flows. The migration is attributed to lift forces on particles that are observed when inertial aspects of the flow become significant. We identified symmetric and asymmetric channel geometries that provide additional inertial forces that bias particular equilibrium positions to create continuous streams of ordered particles precisely positioned in three spatial dimensions. We were able to order particles laterally, within the transverse plane of the channel, with >80-nm accuracy, and longitudinally, in regular chains along the direction of flow. A fourth dimension of rotational alignment was observed for discoidal red blood cells. Unexpectedly, ordering appears to be independent of particle buoyant direction, suggesting only minor centrifugal contributions. Theoretical analysis indicates the physical principles are operational over a range of channel and particle length scales. The ability to differentially order particles of different sizes, continuously, at high rates, and without external forces in microchannels is expected to have a broad range of applications in continuous bioparticle separation, high-throughput cytometry, and large-scale filtration systems.

cell manipulation | Dean flow | filtration | hydrodynamic lift | microfluidics

Continuous manipulation and separation of microparticles, both biological and synthetic, is important for a wide range of applications in industry, biology, and medicine (1–3). Traditional techniques of particle manipulation rely on laminar flow (4) or differences in either particle mobility or equilibrium position in a flow with a variety of externally applied forces (5–7). Recently, microfluidic systems have been shown to be very useful for particle handling with increased control and sensitivity. Systems have been demonstrated that use scale-dependent electromagnetic forces (8–11), microscale hydrodynamic effects (12–14), or deterministic physical interactions and filters (15–17). However, the precision of microfluidic systems based on deterministic interaction with walls or posts may be limited by disturbances from random interparticle contact and spacing, and mechanical systems are prone to clogging. Additionally, throughput for particle manipulation based on external forces has been limited because the time for forces to act decreases with increasing flow rate. Inertial hydrodynamic forces that would increase along with flow rate have, in all but a few cases (18), not been considered in microfluidic systems. This is because of a widely held notion that small length scales require that the Reynolds number (*Re*), a measure of the relative importance of inertial to viscous forces, must be concurrently small, precluding any practically useful inertial effects.

Inertial lift forces on flowing particles have been described in centimeter-scale systems, and they are different in origin than lift forces on bodies in inviscid flows. They were first experimentally reported by Segre and Silberberg (19) for particles flowing through large circular pipes (≈1-cm diameter). In these experiments, following the radial symmetry, scattered flowing particles tended to focus to a narrow annulus at a position 0.6 times the radius of the pipe. No particle manipulation systems were explored based on these macroscale systems primarily because of the large scale of the particles and systems and the difficulty in isolating particles from a focused annulus.

In this work, we use inertial lift forces in laminar microfluidic systems to focus randomly distributed particles continuously and at high rates to a single streamline (Fig. 1*a*), and we exploit particle geometry dependence to develop simple prototype systems for high-throughput separations. We systematically engineer the symmetry of the microchannel systems to reduce focusing of particles from an annulus to four points, to two points, and then to a single point within the channel. In this process, we unexpectedly observed two additional levels of particle ordering, longitudinally along the channel length and rotationally (for asymmetric particles). This process is experimentally determined to be primarily controlled by the ratio of particle size to channel size and the flow characteristics of the system, but it is independent of particle density for the tested range of values. This simple and robust method requires no mechanical or electrical parts, making it ideal for applications ranging from flow cytometry to blood fractionation and no-upkeep continuous filtration systems.

Theoretical Background

Particles suspended in fluids are subjected to drag and lift forces that scale independently with the fluid dynamic parameters of the system. Two dimensionless Reynolds numbers can be defined to describe the flow of particles in closed channel systems (20): the channel Reynolds number (R_c), which describes the unperturbed channel flow, and the particle Reynolds number (R_p), which includes parameters describing both the particle and the channel through which it is translating.

$$R_c = \frac{U_m D_h}{\nu} \quad [1]$$

and

$$R_p = R_c \frac{a^2}{D_h^2} = \frac{U_m a^2}{\nu D_h}. \quad [2]$$

Both dimensionless groups depend on the maximum channel velocity, U_m, the kinematic viscosity of the fluid, $\nu = \mu/\rho$ (μ and ρ being the dynamic viscosity and density of the fluid, respectively), and D_h, the hydraulic diameter, defined as $2wh/(w + h)$

Author contributions: D.D.C., D.I., R.G.T., and M.T. designed research; D.D.C. performed research; D.D.C., D.I., and M.T. analyzed data; and D.D.C., D.I., R.G.T., and M.T. wrote the paper.

The authors declare no conflict of interest.

This article is a PNAS Direct Submission.

*To whom correspondence should be addressed. E-mail: mtoner@hms.harvard.edu.

This article contains supporting information online at www.pnas.org/cgi/content/full/0704958104/DC1.

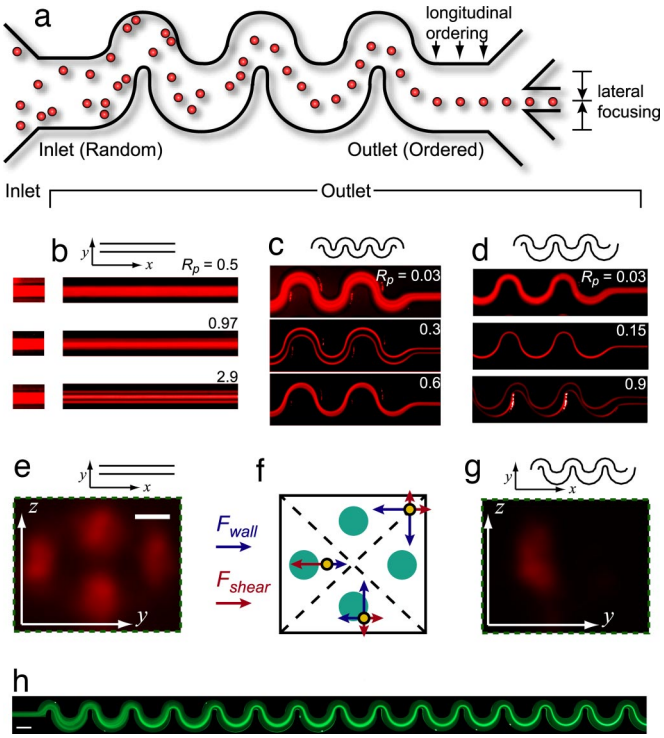

Fig. 1. Inertial self-ordering. (*a*) Schematic drawing of the inertial ordering process. After flowing through a channel of a particular symmetry, precise ordering of initially scattered particles is observed both longitudinally along the direction of flow and laterally across the channel. (*b*) Top-down views of fluorescent streak images of flowing 9-μm-diameter particles in a square channel (50 μm) filled with water (density ρ = 1.00 g/ml and dynamic viscosity $\mu = 10^{-3}$ Pa·s). Flow is from left to right. The inlet region is shown at the left, where the particles are initially uniformly distributed within the fluid. Longer images show the outlet 3 cm downstream for the channel Reynolds number R_c = 15, 30, or 90 (particle Reynolds number R_p = 0.48, 0.97, or 2.9). Focusing of particles into four single streamlines is observed. From above this appears as three lines with double the intensity in the middle streak–line. (*c*) For a symmetric curving channel the symmetry of the system reduces focusing to two streams. Above a critical Dean number (*De*) focusing is perturbed. (*d*) For an asymmetric curving system, focusing down to a single stream is favored. Focusing is again more complex as *De* increases. (*e*) A confocal cross-section of the rectangular channel shown in *b* shows focusing of particles to the four channel faces. (Scale bar, 10 μm.) (*f*) Schematic diagram showing the force balance between the shear-gradient (F_{shear}, red arrows) and wall-induced lift (F_{wall}, blue arrows) for particles in three positions. (*g*) Confocal cross-section for an asymmetric channel. (*h*) Starting at the inlet on the left, a random inlet distribution of fluorescent microparticles is focused to a tight streamline on the right after a short distance. (Scale bar, 160 μm.)

(w and h being the width and height of the channel). The particle Reynolds number has an additional dependence on the particle diameter, a. The definition of Reynolds number based on the mean channel velocity can be related to R_c by $Re = \frac{2}{3} R_c$.

Inertial lift forces dominate particle behavior when the particle Reynolds number is of order 1. Typically, particle flow in microscale channels is dominated by viscous interactions with $R_p \ll 1$. In these systems, particles are accelerated to the local fluid velocity because of viscous drag of the fluid over the particle surface. Dilute suspensions of neutrally buoyant particles are not observed to migrate across streamlines, resulting in the same distribution seen at the inlet, along the length, and at the outlet of a channel. As R_p increases, migration across streamlines has been observed in macroscale systems (19). In a cylindrical tube particles were observed to migrate away from the tube center and walls to form a focused annulus. The theoretical basis for this "tubular pinch" effect was later described to be a combination of inertial lift forces acting on particles at high particle Reynolds numbers (21, 22). The dominant forces on rigid particles are the "wall effect," where an asymmetric wake of a particle near the wall leads to a lift force away from the wall (23), and the shear-gradient-induced lift that is directed down the shear gradient and toward the wall (20). A relation describing the magnitude of these lift forces (F_z) in a parabolic flow between two infinite plates follows from Asmolov (20) and is useful in understanding how the intensity of inertial migration depends on system parameters with, the caveat that the derivation assumes $R_p < 1$.

$$F_z = \frac{\rho U_m^2 a^4}{D_h^2} f_c(R_c, x_c) = \frac{\mu^2}{\rho} R_p^2 f_c(R_c, x_c). \quad [3]$$

Here $f_c(R_c, x_c)$ can be considered a lift coefficient and is a function that is dependent on the position of the particle within the cross-section of the channel x_c and the channel Reynolds number, but independent of particle geometry. At the equilibrium position, where the wall effect and shear-gradient lift balance, $f_c = 0$.

Inertial lift acting on a particle leads to migration away from the channel center. From Eq. **3** an expression for the particle migration velocity, U_p, can be developed assuming Stokes drag, $F_s = 3\pi\mu a U_p$, balances this lift force:

$$U_p = \frac{\rho U_m^2 a^3}{3\pi\mu D_h^2} f_c(R_c, x_c). \quad [4]$$

An estimate of the transverse migration velocity out from the channel center line can be made by using an average value of $f_c \sim 0.5$ for flow through parallel plates (20). This calculation yields a value of 3.5 cm/s for 10-μm particles in a flow with U_m = 1.8 m/s. Traveling a lateral distance of 40 μm requires traveling ≈2 mm downstream in the main flow. Eq. **4** also indicates that the lateral distance traveled will depend heavily on particle diameter, indicating the possibility of separations based on differential migration. Assumptions that limit the accuracy of this analysis are given in the supporting information (SI) *Text*.

Additional interactions between particles and flow have to be considered when channels are not straight. Secondary rotational flow caused by inertia of the fluid itself, called Dean flow (24), has been previously described in curved channels, and can alter the position of flowing particles. Two dimensionless numbers to characterize this secondary flow, the Dean number $\{De = Re(D_h/2r)^{1/2}\}$ and curvature ratio ($\delta = D_h/2r$) can be defined (18, 24), where r is the radius of curvature of the channel. At moderate Dean numbers observed in our experiments ($De < 50$), Dean flow consists of two counterrotating vortices with flow directed toward the outer bend at the midline of the channel and inwards at the channel edges. The magnitude of the rotational flow velocity (U_D) scales as

$$U_D \sim De^2 \nu / D_h. \quad [5]$$

In the presence of other forces (e.g., inertial lift forces) that act to keep a particle in a stationary position, a drag force is applied by the secondary flow with a maximum possible value that is proportional to the secondary flow velocity. From Eq. **5** and assuming Stokes drag, the drag attributable to Dean flow (Dean drag, F_D) scales as $F_D \sim \rho U_m^2 a D_h^2 r^{-1}$.

The balance between inertial lift and Dean drag forces is what determines the preferred location of particles in channels with curved geometry. It should be noted that although lift and drag forces in a simple flow act orthogonally on a body, inertial lift and Dean drag forces may not. This is because inertial lift acts in a perpendicular direction to the primary channel flow, whereas Dean drag is in the direction of the secondary flow, leading both

to be orthogonal to the primary flow. To better understand the overall effect of these forces, it is instructive to compare relative magnitudes at three limiting cases. The ideal condition is where the Dean drag (F_D) is of the same order as the inertial lift (F_z). Here the positional dependence of the Dean drag magnitude can lead to concentration of particles in lift-induced equilibrium positions that interact weakly with the Dean flow (particularly along the channel midline between counterrotating vortices, SI Fig. 5). Particles translating in other strongly interacting locations become unstable. A key point is that the additional force from Dean flow does not create particle focusing, but it acts in superposition with the underlying distribution to reduce the number of equilibrium positions. If $F_D \gg F_z$, then no focusing will be observed as the dominant Dean flow mixes particles, and if $F_D \ll F_z$, then focusing due to inertial lift alone will be observed for channels of sufficient length. With f_c scaling with R_c^n ($n < 0$), following Matas *et al.* (21), the ratio of lift to drag force magnitudes scale as

$$\frac{F_z}{F_D} \sim \frac{1}{\delta}\left(\frac{a}{D_h}\right)^3 R_c^n, \quad (n < 0). \qquad [6]$$

This relation suggests the apparent observation that Dean flow will become irrelevant for the limit as δ approaches 0 (i.e., straight channels), but also suggests a strong third-power dependence on the ratio of particle to channel dimensions. At the same R_c a smaller particle could remain unfocused, irrespective of channel length, because of dominant F_D, whereas a larger particle focuses quickly ($F_z \geq F_D$). Additionally one observes that the ratio decreases and Dean drag becomes more dominant with increasing R_c, suggesting an upper limit on R_c above which all particle sizes will be defocused by mixing due to Dean flow.

Results and Discussion

Inertial Focusing in Rectangular Microchannels. At low flow rates, particles flowing in straight rectangular microchannels are observed to distribute uniformly across the cross-section of the channel. As R_p is increased with increasing fluid velocity, patterns of particle segregation in laminar flow become observable that depend significantly on channel scale and symmetry. First, we show that uniformly distributed particles in rectangular channels migrate across streamlines to four symmetric equilibrium positions at the centers of the faces of the channel and toward the channel edge (Fig. 1 *b* and *e* and SI Movie 1). Particles 9 μm in diameter suspended in water were observed in 50 μm-wide square channels. The degree of focusing increases with R_p (Fig. 1*b*) at a given distance along the channel and also increases with the distance traveled along the channel. For R_p = 2.9 (R_c = 90), complete focusing is observed after a distance of $\approx$1 cm. Focusing differs from previous experiments that observe annuli following the radial symmetry of cylindrical channels. Here the fourfold channel symmetry reduces focusing to four coordinates. The equilibrium position for particles is $\approx$9 μm from the channel edge for R_c = 90 and agrees with theoretical predictions of $\approx$8 μm (20) in an infinite plane system (R_c = 100). This distance is also predicted to move closer to the wall for a given particle size as R_c increases, agreeing with our observations (SI Movie 1). Focusing is experimentally observed at channel faces as opposed to corners despite the symmetric features of corners. Presumably the dominant wall effect acts from two directions on a particle within a corner, and creates an unstable equilibrium point (Fig. 1 *e* and *f*). Inertial lift forces alone allow two-dimensional focusing to four precise positions within the lateral face of a rectangular channel.

Particle Focusing in Curving Microchannels. In curving channel systems symmetry is reduced by additional inertial (centrifugal) forces arising from the particles and fluid. These forces act in superposition with the lift forces to change equilibrium positions of particles flowing within the fluid. The additional inertial forces act in the plus and minus *y* directions in microchannels with a curving *symmetric* geometry. This geometry biases the two stable positions on the sides of the channel and reduces the number of particles collected at the top and bottom focusing points. Experimentally, we observe only two focused lines of particles when the force is sufficient to bias the direction (Fig. 1*c*, SI Movie 2). As R_c increases, mixed streams are again observed, in agreement with an increased contribution from Dean drag that is predicted by Eq. **6**. An *asymmetric* curving geometry leads to further reduction in symmetry of particle focusing. In this case, the net force acts in one direction, biases a single stable position of the initial distribution (Fig. 1 *d* and *g* and SI Movies 3 and 4), and creates a single focused stream of particles. Interestingly, in asymmetric curved channels complete focusing occurs for much smaller $R_p \sim 0.15$ and shorter traveled distances ($\approx$3 mm) than in the case of straight rectangular channels (Fig. 1*h*), which may partly be due to the mixing action of the Dean flow allowing particles to sample the stable regions of the flow more quickly.

We studied the effect of relative particle density on focusing in microchannels. Unexpectedly, when the density of the suspending solution was changed so that the suspended particles were either more or less dense than the solution (i.e., positive or negative buoyancy) focusing was unperturbed and remained at a consistent location (Fig. 2 *a* and *b*). This was further confirmed when particles both less dense (silicone oil, ρ = 0.95 g/ml) and more dense (polystyrene, ρ = 1.05 g/ml) than the suspending fluid (ρ = 1.00

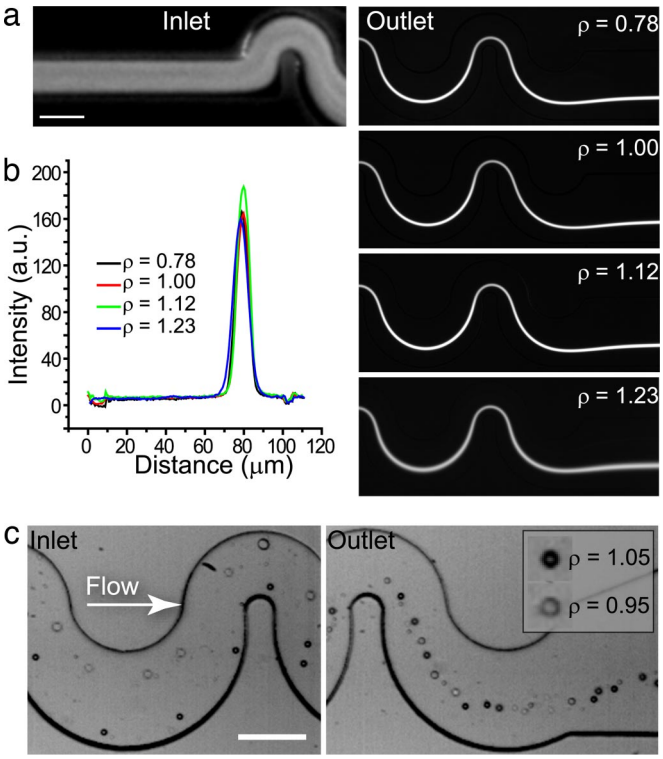

Fig. 2. Density independence of inertial focusing. (a) Polystyrene particles (10-μm diameter, ρ = 1.05 g/ml) initially unfocused were focused when suspended in solutions of both higher and lower density (ρ = 0.78–1.23 g/ml). The R_p in this system is 0.2. (Scale bar, 50 μm.) (*b*) A graph showing intensity cross-sections for these focused streams indicates focusing position is not affected by relative particle density or sign. a.u., Arbitrary units. (c) Particles both more dense (polystyrene, ρ = 1.05 g/ml) and less dense (silicone oil, ρ = 0.95 g/ml) than the suspending solution focus unexpectedly to the same streamline. (Scale bar, 100 μm.)

g/ml), loaded simultaneously, were also found to focus to the same position (Fig. 2*c*). The independence of particle density for particle focusing is not consistent with a dominant centrifugal force acting directly on particles and suggests that Dean drag (F_D) is the dominant effect leading to symmetry reduction. The relative magnitude of the curvature-induced inertial forces are discussed more completely in the *SI Text*.

To characterize the stability and precision of inertially focused streams, a solution of 10-μm polystyrene particles was imaged over 10 min of continuous flow at $R_p = 0.24$. Each image had an exposure time of 700 ms, sampling an average of 1,100 passing particles. The standard deviation of the center position of the focused stream was determined to be 80 nm in the *y* direction (SI Fig. 6) and the focused stream's average width was only 1.05 times the average width of a single particle. Although other external forces, such as magnetic (25), optical (8), and dielectrophoretic (9, 11), may also be used to bias a particular equilibrium positions within the rectangular flow field, an approach using hydrodynamic forces with a curved channel structure is ideal. The additional forces increase with the flow rate, and only a minor geometric change is required to focus particles, with no additional mechanical or electrical parts.

In addition to the focusing of particles across the transverse plane of the channel, self-ordering of particles in the longitudinal direction, along the flow lines has been observed. We used high-speed imaging (2-μs exposure) to reveal characteristic long trains of particles (10–15 particles) with uniform spacing that alternated between the four stable lateral positions in rectangular channels (Fig. 3 *a* and *b*, SI Movie 5) or were concentrated in a single stream for the asymmetric channels (Fig. 3 *c* and *d*). The key result here is that particle–particle distances below a threshold are not favored, and self-ordering in a longitudinal direction results. A shorter preferred distance is observed at higher R_c in rectangular channels than in asymmetric curved channels (see autocorrelation functions in Fig. 3 *b* and *d*). Ordered particle trains have been observed in comparable macroscale systems, where it has been postulated that preferred distances may arise from the interaction of secondary flows around rotating particles in a shear flow (26). In this case the detached secondary flow itself may act as an object. In the previous work rigid particles (≈0.5-mm diameter) in large (≈1-cm diameter) cylindrical tubes were found to form long trains above $R_c \sim 450$ with stable interparticle spacing decreasing with R_p. In our system we observed robust ordering for a lower $R_c \sim 90$. We then evaluated the throughput of the system, where the shortest time between frames was limited to 10 μs for a 32 × 32 pixel image. For this small image size, focusing of particles to the detection point is essential for increased throughput. Because rectangular channels were not limited to a maximum flow rate, we used them for ordered high-throughput imaging of both 10-μm particles (SI Fig. 7 and SI Movie 5) and cells (SI Fig. 8 and SI Movie 6). A histogram of distances between particles (SI Fig. 7*c*) shows that self-ordering allowed ~30,000 particles per second to be imaged, with only 5% of particles displaying center-to-center distances <16 μm.

Cell Focusing in Microchannels. We observed similar self-ordering for cells in diluted (2% vol/vol) whole blood as for particles in buffer solutions (Fig. 3 *f* and *g*). Deformable particles such as cells may experience additional hydrodynamic forces in the applied flow field (22, 27); however, from our experimental results whole blood, droplets, and cultured cells were found to behave as rigid particles in straight and curving microchannels. Additionally, a remarkable fourth dimension of ordering was observed when discoid red blood cells aligned rotationally such that the disk axis was parallel to the rectangular channel wall (Fig. 3 *f* and *g* and SI Movie 6). Images at a rate of ≈15,000 cells per second were obtained in this system (SI Fig. 8).

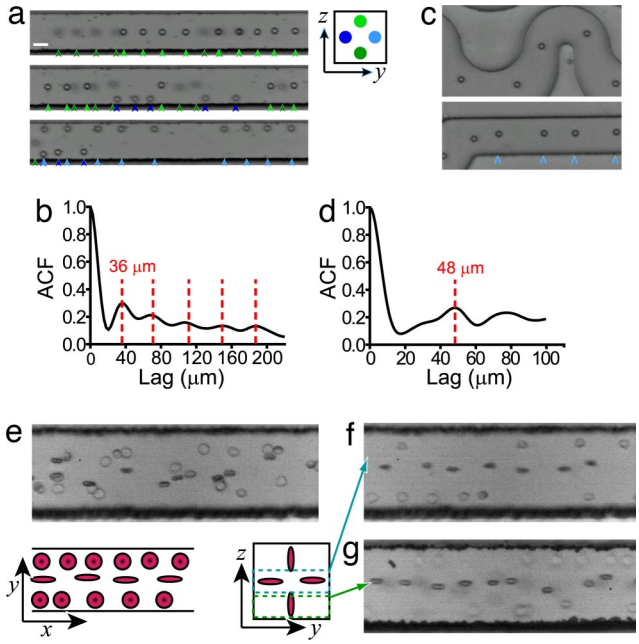

Fig. 3. Longitudinal and rotational inertial self-ordering. (*a*) Three high-speed images (2-μs exposure) are shown, demonstrating ordered particle trains at the four positions of equilibrium. Particles are 10 μm in diameter and the flow is at $R_c = 120$. Colored arrows below the images indicate particles at specific positions in the *y*–*z* plane that correspond to the legend. Trains tend to alternate between the positions instead of occupying several coincidently. (Scale bar, 20 μm.) (*b*) An autocorrelation function (ACF) confirms particle ordering with an average distance of 36 μm. (*c* and *d*) For an asymmetric curved channel, ordering occurs with a larger average displacement of 48 μm. (*e*) For $R_c = 0.3$, high-speed images of dilute whole blood show random distributions and random rotational alignment of red blood cells within a 50-μm channel. (*f*) At $R_c = 60$ a high-speed image with the focus at the midplane of the channel reveals characteristic trains of red blood cells at the top and bottom of the image. Rotational alignment of these cells is observed with the disk axis parallel to the wall. (*g*) Focusing at the bottom of the channel for the same R_c reveals trains of red blood cells with a similar alignment of the disk axis to the nearest wall, consistent with symmetry.

We observed no significant alterations in cell viability after they passed through the inertial focusing systems at high speeds. Even at average velocities of 0.5 m/s there was no discernable damage to cells (99.0% vs. 99.8% initial viability as measured by using a fluorescent live/dead assay). High cell viability and throughput are critical for applications such as flow cytometry. With inertial self-ordering, clear advantages emerge compared with hydrodynamic focusing used in current flow cytometers. These include (*i*) a single stream input, (*ii*) reduction of multiple cells in the interrogation spot because of longitudinal self-ordering, and (*iii*) angular orientation of nonspherical particles for uniform scatter profiles. Another powerful advantage of this focusing system is that throughput can be easily scaled by parallel channels (SI Fig. 9 and SI Movie 4) because additional fluidic channels for the sheath fluid are not required. Possible drawbacks of the technique include the need to control the flow rate within an optimal range to have successful focusing, and the dependence on particle size.

Differential Focusing for Separation Applications. Applications in separation stem directly from the differential focusing of particles of different sizes. We experimentally observed various levels of focusing for cells and particles of different sizes. To investigate these effects in more detail, a range of particle diameters (2–17 μm) and channel sizes (D_h = 10–87 μm) were tested over a range R_c = 0.075–225 for curving asymmetric channels. The focusing

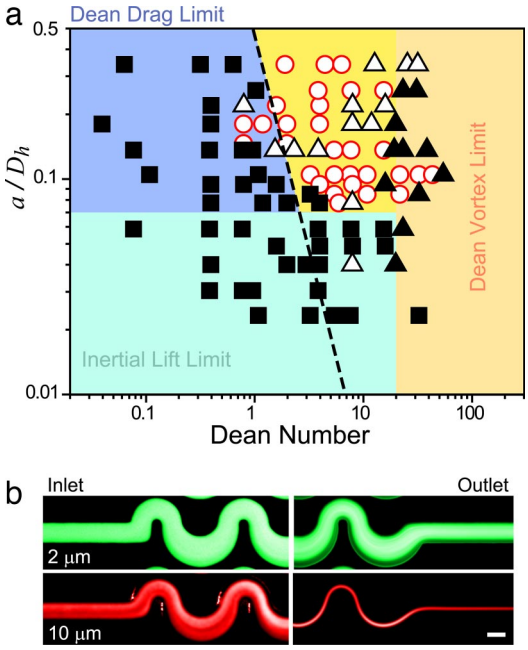

Fig. 4. Size dependence of particle ordering. (*a*) Results for focusing to a single streamline as a function of the Dean number of the flow and the ratio of particle diameter to channel hydraulic diameter (a/D_h) are plotted. No focusing or focusing to four streams corresponds to filled squares, focusing to two streams corresponds to open triangles, focusing to a single stream is represented by open circles, and more complex behavior is shown as filled triangles. Data for this graph were collected by using various-sized particles and channel geometries with a fixed length of 3 cm. Different regimes for successful focusing are defined by interaction of Dean drag (F_D) and inertial lift (F_Z) across the parameter space. The broken line represents a line of constant Dean drag of 0.5 nN. (*b*) Differential focusing of 10- and 2-μm mixed particles in water. The 2-μm particles remain unfocused after transiting 3 cm of asymmetric turns, whereas 10-μm particles are sharply focused. R_c = 7.5. (Scale bar, 50 μm.) Fractions of the stream can be collected to obtain ideally pure smaller particles and enriched populations of larger particles at high throughput.

results were plotted as a function of De and the ratio a/D_h (Fig. 4*a*). In addition, the lateral distance traveled in a straight rectangular channel at constant R_c can theoretically be shown to increase with a/D_h cubed, yielding kinetic separations (SI Fig. 10). For an asymmetric system, the additional effects due to Dean flow act along with inertial lift to shape the allowable range of particles and channel dimensions for successful focusing of particles into single streams. From the experimental data and theoretical calculations a large region for successful particle focusing can be defined where $a/D_h > 0.07$. Below this value two effects scaling with a/D_h may result in a loss of focusing: (*i*) inertial migration [scaling with $(a/D_h)^3$] is slower than what is required for complete focusing in the given length of channel; or (*ii*) following from Eq. **6**, Dean drag becomes much larger than inertial lift for all values of R_c as a/D_h becomes small. Another limit is seen for $De > 20$; above this level, drag from Dean vortices is larger than the inertial lift forces for most particle sizes (see dependence on R_c in Eq. **6**) and leads to particle mixing. Still, sufficient Dean flow is necessary to bias particular equilibrium points (a line of constant average Dean drag is drawn with the value $F_D = 0.5$ nN). Last, a practical limit is seen for $a/D_h > 0.5$, where particle obstruction of the channels may occur.

The data plotted in Fig. 4*a* appear similar to a phase diagram and are critical for determining the correct design conditions for particle separation. The correct use of this diagram is dependent on particles reaching equilibrium states in the given channel length, where focusing behavior is not kinetic in origin. A vertical movement on the diagram corresponds to changing particle size if channel geometries are held constant. To effect a separation, one must choose a region in the phase diagram (i.e., a specific geometry) where a small change in particle size leads to a change from a focused to an unfocused stream. Thus one particle size is focused to a particular streamline and can be collected as an enriched fraction, whereas the other, smaller, particles are unfocused. Ideally pure fractions can be collected through the use of multiple outlets (Fig. 4*b* and SI Movie 7).

High-throughput separations are possible with these systems because of the high R_c at which they operate (SI Fig. 11 *c* and *d*). For a flow rate of 1.5 ml·min^{-1} of 1% particle solution a mass sorting rate of $\approx$1 g·hr^{-1} is achieved for an unoptimized device that covers an area of 1.6 cm^2. Particles close in size (4 and 7 μm) can also be separated by tuning the asymmetric channel geometry (SI Fig. 11 *a* and *b*), although with slightly less throughput. In these systems there are no externally applied forces other than the pressure to drive the flow, and therefore it is straightforward to cascade and parallelize these design elements to enhance enrichment and throughputs to very high levels, or combine elements with different hydraulic diameters to separate across more than one size threshold (15, 16). Previous microfluidic systems have been shown to be very accurate in resolving particles of different sizes with lower throughputs. Typical of most microfluidic systems, a throughput of 30 mg·hr^{-1} was described for deterministic displacement (15) with a device area of 15 cm^2. In applications dealing with small samples these throughputs can be more than adequate; however, for applications in rare cell cytometry and purification or industrial filtration increased throughput is essential.

Conclusions

In this work we communicate several nonintuitive phenomena that yield different levels of ordering on flowing particles in microchannel systems. We identify ranges of parameters that allow for utilization of the phenomena and suggest key physical principles and forces that are likely responsible for this ordering. Applications of these phenomena are diverse, and a theoretical understanding of the interaction of particles with inertial flows in complex systems may yield further insight. The particular geometries presented here could be adopted immediately and should provide a significant improvement over current sheath-flow-based focusing methods in a variety of particle counting and sizing instrumentations. Applications in separation and filtration are also significant because throughput is comparable to macroscale systems and mechanical obstruction of sieve-based filters is avoided. The work should be applicable not only in microscale systems but also in macroscale systems. Overall, this inertial focusing process is continuous and high-throughput and does not require external forces. These features are highly compatible with broad uses in cell and other bioparticle sorting, high-throughput flow cytometry, and industrial filtration.

Materials and Methods

Materials. Fluorescent polystyrene microparticles ($\rho \sim 1.05$ g/ml) were purchased from Bangs Laboratories and Duke Scientific. For 4 (3.87)-μm and 7 (7.32)-μm particles the Bangs Laboratories product codes were FS05F/7772 and FS06F/6316, respectively. For 2 (2.0)-μm, 3 (3.1)-μm, 9-μm, 10 (9.9)-μm, and 17-μm particles the Duke Scientific product numbers were R0200, G0300, 36-3, G1000 and 35-4. Particles were mixed to desired weight fractions by dilution in PBS and stabilized by addition of 0.1% Tween 20. In the various described experiments particle wt/vol % varied between 0.1% and 1%. Silicone oil droplets were formed from 10% wt/vol DC 200 (10 centistokes, Dow Corning) stabilized with 2% wt/vol polyethylene glycol monooleate (molecular weight 860, Sigma–Aldrich). The mixture was shaken vigorously and allowed to settle for 20 min. Solution was taken from the bottom 1 cm of the vial to

ensure a size range of droplets <20 μm. Solutions of different densities were prepared from ethanol (ρ = 0.78 g/ml) or concentrated $CaCl_2$ solutions (ρ = 1.12 and 1.23 g/ml); viscosities of these solutions varied from 1 to 3 centipoise.

Cells (H1650) cultured in RPMI medium 1640 with 10% FBS were trypsinized and resuspended in PBS before use. Blood was collected from a healthy volunteer in Vacutainer tubes by a trained phlebotomist and diluted in PBS to 0.5–5% for experiments. Cells were dyed with either calcein AM (5 μM) or Hoechst 33342 (1 μM).

Experimental Methods and Notes. Further methods and notes are included in the *SI Text* available online.

We thank Octavio Hurtado for his assistance with microfabrication, Shannon Stott for assistance with high-speed imaging, and Jon Edd for silicone oil droplets. We thank an anonymous reviewer for key insights in the theory section. This work was supported in part by the National Institute of Biomedical Imaging and Bioengineering (BioMEMS Resource Center, P41 EB002503) and an American Cancer Society Postdoctoral Fellowship.

1. Giddings JC (1993) *Science* 260:1456–1465.
2. Nolan JP, Sklar LA (1998) *Nat Biotechnol* 16:633–638.
3. Toner M, Irimia D (2005) *Annu Rev Biomed Eng* 7:77–103.
4. Kachel V (1976) *J Histochem Cytochem* 24:211–230.
5. Fuh CB (2000) *Anal Chem* 72:266A–271A.
6. Giddings JC (1992) *Sep Sci Technol* 27:1489–1504.
7. Schaflinger U (1990) *Fluid Dyn Res* 6:213–249.
8. MacDonald MP, Spalding GC, Dholakia K (2003) *Nature* 426:421–424.
9. Choi S, Park J-K (2005) *Lab Chip* 5:1161–1167.
10. Hu XY, Bessette PH, Qian JR, Meinhart CD, Daugherty PS, Soh HT (2005) *Proc Natl Acad Sci USA* 102:15757–15761.
11. Yu CH, Vykoukal J, Vykoukal DM, Schwartz JA, Shi L, Gascoyne PRC (2005) *J Microelectromech Syst* 14:480–487.
12. Yamada M, Seki M (2005) *Lab Chip* 5:1233–1239.
13. Huh D, Bahng JH, Ling Y, Wei H-H, Kripfgans OD, Fowlkes JB, Grotberg JB, Takayama S (2007) *Anal Chem* 79:1369–1376.
14. Yang S, Undar A, Zahn JD (2006) *Lab Chip* 6:871–880.
15. Davis JA, Inglis DW, Morton KJ, Lawrence DA, Huang LR, Chou SY, Sturm JC, Austin RH (2006) *Proc Natl Acad Sci USA* 103:14779–14784.
16. Huang LR, Cox CC, Austin RH, Sturm JC (2004) *Science* 304:987–990.
17. Sethu P, Sin A, Toner M (2006) *Lab Chip* 6:83–89.
18. Sudarsan AP, Ugaz VM (2006) *Proc Natl Acad Sci USA* 103:7228–7233.
19. Segre G, Silberberg A (1961) *Nature* 189:209–210.
20. Asmolov ES (1999) *J Fluid Mech* 381:63–87.
21. Matas JP, Morris JF, Guazelli E (2004) *Oil Gas Sci Technol* 59:59–70.
22. Leal LG (1980) *Ann Rev Fluid Mech* 12:435–476.
23. Zeng L, Balachandar S, Fischer P (2005) *J Fluid Mech* 536:1–25.
24. Berger SA, Talbot L (1983) *Annu Rev Fluid Mech* 15:461–512.
25. Inglis DW, Riehn R, Austin RH, Sturm JC (2004) *Apl Phys Lett* 85:5093–5095.
26. Matas JP, Glezer V, Guazelli E, Morris JF (2004) *Phys Fluids* 16:4192–4195.
27. Faivre M, Abkarian M, Bickraj K, Stone HA (2006) *Biorheology* 43:147–159.